Published in final edited form as:
Cancer Res. 2008 June 15; 68(12): 4649–4657. doi:10.1158/0008-5472.CAN-07-6003.

Endothelial Function of *von Hippel-Lindau* Tumor Suppressor Gene: Control of Fibroblast Growth Factor Receptor Signaling

Kristen J. Champion, **Maria Guinea**, **Vincent Dammai**, and **Tien Hsu**
Department of Pathology and Laboratory Medicine and Hollings Cancer Center, Medical University of South Carolina, Charleston, South Carolina

Abstract

von Hippel-Lindau (VHL) disease results from germline and somatic mutations in the *VHL* tumor suppressor gene and is characterized by highly vascularized tumors. *VHL* mutations lead to stabilization of hypoxia-inducible factor (HIF), which up-regulates proangiogenic factors such as vascular endothelial growth factor (VEGF). This pathway is therefore believed to underlie the hypervascular phenotypes of the *VHL* tumors. However, recent studies have identified novel *VHL* functions that are independent of the HIF-VEGF pathway. In addition, a potential role of *VHL* in the tumor microenvironment, which carries heterozygous *VHL* mutations in VHL patients, has been overlooked. Here, we report a novel HIF-independent *VHL* function in the endothelium. *VHL* knockdown in primary human microvascular endothelial cells caused defective turnover of surface fibroblast growth factor (FGF) receptor, increased extracellular signal-regulated kinase signaling, and ETS1 activation, leading to increased cell motility in response to FGF and three-dimensional cord formation *in vitro*. HIF-α knockdown in *VHL* loss-of-function endothelial cells does not impede their elevated *in vitro* angiogenic activity. Importantly, the elevated angiogenic response to FGF is recapitulated in *Vhl*-heterozygous mice. Thus, partial loss of function of *VHL* in endothelium may be a contributing factor in tumor angiogenesis through a HIF-VEGF–independent mechanism.

Introduction

The von Hippel-Lindau (VHL) disease is a multiple tumor syndrome resulting from inactivation of the *VHL* tumor suppressor gene on chromosome 3p25 (1–3). The disease is characterized by development of highly vascularized benign and malignant tumors, including retinal and central nervous system hemangioblastoma, pheochromocytoma, and clear-cell renal cell carcinoma (RCC). The VHL protein (pVHL) has been shown to function as an E3 ubiquitin ligase (4–6). Prominent among its targets are the α subunits of the hypoxia-inducible factor (HIF; refs. 3,7–9). Because HIF directly activates angiogenic factors, such as vascular endothelial growth factor (VEGF), it is widely accepted that the constitutively activated HIF activity in *VHL* mutant tumor cells can account for the hypervascular phenotypes in the VHL disease.

However, there is increasing evidence to suggest that pVHL has multiple cellular functions besides being a negative regulator of HIF-α (10). Among them, loss of *VHL* function is known to result in dysregulation of cytoskeletal organization and ECM assembly (11–13). Some of these defects have been found to correlate with a well-documented *VHL* mutant phenotype of

Requests for reprints: Tien Hsu, Pathology and Laboratory Medicine, Hollings Cancer Center, Medical University of South Carolina, 86 Jonathan Lucas Street, Room 330, Charleston, SC 29425. Phone: 843-792-0638; Fax: 843-792-5002; E-mail: E-mail: hsut@musc.edu.

Disclosure of Potential Conflicts of Interest
No potential conflicts of interest were disclosed.

increased cell motility (12,14,15). In our previous studies, we showed that *VHL* null RCC-derived cells exhibit elevated motility and that this phenotype is at least in part the result of cell surface accumulation of fibroblast growth factor (FGF) receptor 1 (FGFR1) and enhanced signaling via extracellular signal-regulated kinase 1/2 (ERK1/2) (16).

It is worth noting that the majority of VHL disease studies have focused on *VHL* mutations within tumor cells and have often overlooked the fact that all VHL patients are heterozygous mutants for all somatic cells. It is tempting to contemplate the possibility that partial loss of function of *VHL* in the stroma, including the endothelium, may contribute to the hypervascular phenotype. Indeed, recent evidence supports this notion. For example, conditional *Vhl* knockout in the endothelial cells resulted in embryonic lethality with vascular defects similar to those in *Vhl* homozygotes (17). Also, it has been shown that mice carrying one allele of germline *VHL* null mutation (i.e., heterozygous mice) developed blood vessel tumors of the liver that are comparable or more severe than vascular tumors resulting from specific homozygous conditional knockout in the hepatocytes (18). Additional studies have confirmed that *VHL* heterozygocity can predispose mice to develop severe vascular lesions (19), although the exact mechanism is unclear. In this report, we show that partial loss of *VHL* function in matured endothelial cells confers elevated angiogenic activity via up-regulated FGFR signaling.

Materials and Methods

Cell lines and reagents

VHL$^+$ primary human microvascular endothelial cells (HMVEC) isolated from neonatal skin were from Cambrex. Cells were maintained in endothelial cell basal medium (Cambrex) supplemented with 5% fetal bovine serum + SingleQuots cytokine and growth factor supplement kit from Cambrex. Cells were used within eight to nine passages and grown in culture dishes coated with bovine type I monomeric collagen solution (from Inamed Biomaterials). Transfection of HMVECs was performed by electroporation, which consistently achieved ~ 80% transfection efficiency. PD98059 inhibitor and Akt inhibitor V, Triciribine, are from Calbiochem.

RNA interference

Plasmid-based short hairpin RNAs (shRNA) were constructed as follows: target sequences (VHL shRNA-I, gagaactgggacgaggccg; VHL shRNA-II, gctgcccgtatggctcaac; HIF-1α shRNA, aacgacacagaaactgatgac; and control, random sequence) were cloned into pCDNA-based plasmid downstream of U6 promoter. Validated FGFR2 small interfering RNA (siRNA) and control siRNA were obtained from Santa Cruz. Both VHL and HIF-1α specific siRNA targets have been used successfully (16,20,21). AdEts1 siRNA vector and the control virus carrying random oligo sequence are a kind gift from Dr. Maria Trojanowska, Medical University of South Carolina. AdEts1 siRNA target sequence is cagacaccttgcagaatga.

Scratch assay

HMVECs were grown to 90% confluency in collagen-coated six-well plates and scratched with a 1,000-μL pipette tip. Fresh complete EBM2 medium was added, and wound-healing was followed for 24 h. Cell proliferation was monitored by staining of cells with rabbit polyclonal Ki-67 proliferation marker (Abcam). Assay was performed in triplicate, and the results were analyzed using Student's *t* test.

Transwell migration assay

Transwell chamber (Corning; 24-well 8-μm pore size) assays were performed using 2×10^4 cells per insert seeded into the upper chamber in 1% serum and no growth factor supplements. The bottom chamber contained low serum (1%) alone, low serum + basic human recombinant FGF (Promega) + 2.5 μg/mL heparin (Sigma), or low serum + human recombinant $VEGF_{165}$ (BD Biosciences) + 2.5 μg/mL heparin (Sigma). Migration was followed over 24 h. Inserts were rinsed in 1× PBS, and cells on the upper side were removed with a cotton swab. Migrated cells attached to bottom side were stained with crystal violet and counted using a 10× objective focused at the center. Results were analyzed using Student's t test.

Three-dimensional *in vitro* angiogenesis assay

The assay followed the previously described protocol (22,23) with modifications. Monolayers of HMVECs (~ 80% confluency) grown on collagen-coated LabTek chambered slides were overlaid with a 1-mm layer of collagen type I gel followed by a second 3-mm collagen-Matrigel layer (3:1) mixed with indicated numbers of primary human dermal fibroblasts. Growth Factor Reduced BD Matrigel Matrix was obtained from BD Biosciences. Complete EBM-2 medium was then added to the chambers. The medium was refreshed after 48 h, and cord formation was observed using light and fluorescent microscopy after 72 h. Cord formation was quantified using NIH ImageJ software to measure total cord length per field. Assay was performed in triplicate chambers for each condition. Statistical analysis was performed using Student's *t* test. For mitogen-activated protein kinase kinase (MAP/ERK kinase 1) inhibitor (25 μmol/L) or Akt inhibitor V (10 μmol/L) treatments, the inhibitor was applied to monolayer of serum-starved endothelial cells at the indicated concentration for 2 h before addition of collagen layers. Complete media containing inhibitor was then added to chambers after gel overlay and refreshed every 8 h.

Western blotting and antibodies

Western blotting was according to standard procedures. All antibodies were used at recommended dilutions. Mouse monoclonal antibodies are doubly phosphorylated ERK1/2 (dp-ERK; Sigma), β-actin (Sigma), VHL (Neomarkers and Cell Signaling), HIF-1α (Novus Biologicals), phosphothreonine (Zymed), and phosphoserine (Zymed). Rabbit polyclonal antibodies are FGFR2 (Santa Cruz), ERK1/2 (Sigma), Akt (Cell Signaling), phosphorylated Akt (Cell Signaling), ETS1 (Santa Cruz), epidermal growth factor receptor (EGFR; Sigma), and VEGF receptor 2 (VEGFR2; Calbiochem). Secondary antibodies used were HRPO-conjugated antimouse IgG (Sigma) and antirabbit IgG (Sigma).

Immunohistochemistry

Cells were fixed in PBS + 4% paraformaldehyde for 30 min, quenched with PBS + 20 mmol/L Tris-HCl (pH 7.6), and permeabilized with 0.2% Saponin (Sigma) for 15 min at room temperature. Incubation with respective primary and secondary antibodies was done in PBS + 1% bovine serum albumin (BSA) for 1 h at room temperature. Primary antibodies (p-FGFR and VHL from Cell Signaling and LAMP1 from Developmental Studies Hybridoma Bank, University of Iowa) were used at 1:100 dilution. Secondary antibodies used were antimouse-Alexa 546, antirabbit-Alexa 546, antimouse-Alexa 633, and antirabbit-Alexa 633 at 1:200 dilutions. Confocal images were acquired with Olympus IX70 (Fluoview 300).

Cell surface biotinylation

Cells grown in six-well plates were washed with ice-cold PBS (pH 7.4) and incubated with 0.5 mL/well PBS containing 0.5 mg/mL sulfo-NHS-LC-Biotin (Pierce) for 30 min at 4°C. After washing and free cross-linker quenching in PBS + 50 mmol/L Tris-HCl (pH 7.0), cells were lysed with 300 μL/well of 1% Triton–radioimmunoprecipitation assay buffer (RIPA)

containing protease inhibitors (Roche). After protein estimation (Pierce BCA), 1.5 mg extracts were incubated with NeutrAvidin Biotin-Binding Protein (Pierce) overnight at 4°C. After washing in RIPA buffer, samples were eluted by boiling in 1× SDS sample buffer and blotted with indicated antibodies to detect surface receptor fraction. A portion of total input lysate was reserved for detection of total levels of receptors.

Activated receptor chase

Recombinant human basic FGF (bFGF; 400 ng/mL; Promega) was mixed with 2.5 μg/mL heparin (Sigma) in serum-free media (with 1% BSA) and added to serum-starved cells (6 h) grown on glass coverslips coated with monomeric collagen. Cells were incubated at 4°C for 2 h to allow ligand-receptor engagement, washed with cold plain EBM-2, and chase initiated in prewarmed plain EBM-2 (37°C) for indicated times. Coverslips were lifted and directly fixed in PBS + 4% formaldehyde and stained using indicated antibodies.

Animals

Vhl knockout mice (*129S;ICR-Vhlh*$^{tm1Bjg/J}$) are homozygous lethal as described (24) and were obtained from The Jackson Laboratory. Experiments were performed on 8-wk-old to 11-wk-old animals, using the wild-type animals from the same litter as a control. Genotyping followed the instructions provided by the vendor. Animal housing and all experimental procedures were conducted in accordance with current regulations by Institutional Animal Care and Use Committee of Medical University of South Carolina.

In vivo subcutaneous angiogenesis assay

Heparin (25 μg/mL; from Sigma) was mixed with bFGF (2.5 μg/mL) in PBS and incubated on ice for 1 h before the solution was diluted 10× into the Matrigel matrix (BD Matrigel Growth Factor Reduced; BD Biosciences). Mice (ages 8–11 wk) were anesthetized, and 0.5 mL of Matrigel solution was injected in the subcutaneous tissue of the abdominal wall. The opposite side was used as a control (Matrigel without bFGF and heparin). After a 7-d incubation, mice were anesthetized and infused by intracardiac injection with 0.3 mL of fluorescein-isothiocyanate-dextran (FITC-dextran; from Sigma) at 50 mg/mL. The FITC-dextran was allowed to perfuse through the vascular system for 10 min. After euthanasia, the Matrigel plug was removed and the resulting neovessel formation was analyzed by fluorescence microscopy. The images were quantified using NIH ImageJ. Results were analyzed by Student's *t* test.

Isolation of mouse kidney endothelial cells

Endothelial cells were isolated from kidney cortex of *Vhl*$^{+/-}$ mice or the wild-type littermates by immunomagnetic purification with anti–CD-31 loaded immunobeads (Dynal) as previously described (25–27). Both cell lines were exposed to three rounds of immunopurification and verification for endothelial markers CD31 and von Willebrand factor (vWF) before experimentation.

Results

VHL knockdown HMVECs exhibit increased cell motility

The potential endothelial function of pVHL was assessed in primary HMVECs isolated from neonatal skin. As shown in Fig. 1*A*, expression of *VHL* shRNA, but not control shRNA (scrambled), resulted in significant reduction in pVHL levels.

"Scratched wound-healing" and transwell migration assays were used to quantify the migratory properties of *VHL*$^{+}$ and *VHL* knockdown HMVECs. In wound-healing experiments, *VHL* knockdown cells filled ~ 80% of a ~ 500-μm wound within 24 hours, whereas *VHL*$^{+}$ cells filled

only 40% of the wound (Fig. 1*A*). Importantly, cell proliferation was found to be similar in VHL^+ and *VHL* knockdown HMVECs (stained with Ki-67; data not shown), suggesting that the observed wound healing results are due to differences in migratory abilities of the cells.

Quantitative analysis of three-dimensional chemotactic migration was assessed using transwell migration assays (Fig. 1*B*). First, the intrinsic migratory abilities of VHL^+ and *VHL* knockdown cells were assessed using low serum media in the upper and bottom chambers. Next, chemotactic migration toward a proangiogenic stimulus was assessed by adding either of the two major angiogenic factors, bFGF or VEGF, in the bottom chamber. Dosage response of *VHL* knockdown HMVECs was first established over the concentration range used in various published reports (Supplementary Fig. S1; refs. 28,29). Optimal dosages (400 ng/mL bFGF and 200 ng/mL VEGF) were chosen for the assays shown in Fig. 1*B*. Compared with VHL^+ HMVECs, *VHL* knockdown HMVECs exhibited significantly increased intrinsic, as well as FGF-stimulated, cell migration ($P \leq 0.05$). Interestingly, although VEGF could stimulate migration of both VHL^+ and *VHL* knockdown cells, there is no statistically significant difference in their responsiveness to VEGF ($P = 0.36$). Taken together, *VHL* knockdown in HMVECs leads to increased migratory ability, which is further preferentially induced by bFGF.

VHL knockdown HMVECs exhibit increased angiogenic activity *in vitro*

We next assessed the angiogenic potential of *VHL* knockdown HMVECs using an established three-dimensional *in vitro* angiogenesis assay (22,23), as diagrammed in Fig. 1*C*. In this assay, HMVECs are first cultured in collagen I–coated wells to ~ 80% confluency before a 1-mm layer of collagen I gel was laid over the monolayer. If cultured alone, the HMVECs remain as a monolayer and barely penetrate the collagen gel (data not shown). However, in the presence of supporting cells, such as primary human dermal fibroblasts embedded in another 3-mm gel layer atop the 1-mm acellular layer, HMVECs migrate into the gel and form cord-like structures. We first tested the cord-forming capability of VHL^+ and *VHL* knockdown HMVECs under optimal conditions, i.e., in the presence of "high amount" (3.75×10^4 cells in 0.6 mL) of fibroblasts (22). Whereas both VHL^+ and *VHL* knockdown HMVECs migrated into the matrix and formed vessel-like cords, *VHL* knockdown HMVECs formed a significantly (~ 40%) greater amount of cords (Fig. 1*D*). For additional experimental support, this assay was repeated using a second *VHL* shRNA construct and similar results were observed (Supplementary Fig. S2).

The "high amount" of fibroblasts used above might mask intrinsic differences in HMVEC activity due to the abundant angiogenic factors supplied by the large number of fibroblasts. Therefore, to test if *VHL* knockdown cells are more responsive to limited angiogenic stimuli, the cord formation assays were performed in the presence of suboptimal amount of fibroblasts (1.5×10^4 cells in 0.6 mL). Under this condition, VHL^+ HMVECs could no longer penetrate the collagen gel whereas *VHL* knockdown HMVECs were still able to invade the gel and organize into cords (Fig. 1*D*), suggesting that they are more sensitive and responsive to the reduced proangiogenic signals.

Cell surface accumulation of FGFR in *VHL* knockdown HMVECs

We have previously shown that *Drosophila VHL* negatively regulates migration of the tracheal tubule cells, a developmental model for mammalian angiogenesis (30). We have also shown that abnormal accumulation of FGFR on cell surface resulting from defective endocytosis leads to aberrant cell migration in *Drosophila* trachea and in renal carcinoma cells (16,31,32). Because our results indicated that *VHL* knockdown HMVECs exhibited an elevated response to bFGF (Fig. 1*B*), we examined whether a similar mechanism involving up-regulation of FGFR signaling is responsible for mediating the motility in HMVECs. We indeed observed increased surface accumulation of activated FGFR (tyrosine 653/654–phosphorylated FGFR)

in *VHL* knockdown HMVECs compared with *VHL*$^+$ HMVECs (Fig. 2*A*). The result was also verified using a second *VHL* shRNA construct (Supplementary Fig. S3).

The differential membrane accumulation of FGFR was confirmed by surface biotinylation assay. As shown in Fig. 2*B*, while total cellular levels of FGFR2 remain unchanged with or without *VHL*, knockdown of *VHL* leads to a 3-fold increase of surface FGFR2. Note that FGFR1 is expressed at very low levels in these cells (data not shown). Interestingly, surface levels of VEGFR2 are unchanged. We also noted that EGFR levels are higher on the surface of *VHL*$^+$ cells compared with *VHL* knockdown cells. This intriguing phenomenon has been observed in cultured renal carcinoma cells (16), although its physiologic significance remains unclear.

VHL regulates endocytosis of activated FGF receptors

Defective endocytosis of FGFR can result in surface retention, leading to prolonged signaling and increased cell migration and invasion in both human and *Drosophila* (16,31–33). To test if this occurs in *VHL* knockdown HMVECs, ligand-stimulated endocytosis of activated FGFR was synchronized and followed over time. Serum-starved cells were incubated with bFGF + heparin at 4°C for 2 hours and then chased with ligand-free media at 37°C (Fig. 2*C*). Five minutes after initiation of chase, activated FGFR (p-FGFR) is visible at or near the cell surface (denoted by arrows) in both *VHL*$^+$ and *VHL* knockdown cells. By 20 min after initiation of chase, p-FGFR is mostly internalized into intracellular vesicles (denoted by arrowheads) in the *VHL*$^+$ cells. At this time point, many of these p-FGFR–containing vesicles also stain positive for the late endosome/lysosome marker, LAMP1 (Fig. 2*D*, *top left*), consistent with the notion that the internalized FGFR is targeted for degradation. pVHL is seen associated with some but not all of the p-FGFR–containing vesicles (Fig. 2*D*, *top right*), indicating that pVHL is only associated with p-FGFR in part of the endocytic pathway, perhaps only in the early endosomes. Indeed, pVHL is excluded from the LAMP1-containing vesicles (Fig. 2*D*, *bottom*). At 40 min, most of the internalized p-FGFR is degraded in *VHL*$^+$ cells (Fig. 2*C*). This time course is consistent with the normal kinetics of endocytic process of activated receptor tyrosine kinases (34). In contrast, at 20 and 40 min after receptor chase in *VHL* knockdown cells, p-FGFR is still present on the cell surface (arrows in Fig. 2*C*, *bottom*), indicating defective internalization of p-FGFR in *VHL* knockdown HMVECs.

FGFR2 and ERK activities regulate motility in *VHL* knockdown HMVECs

We next sought to verify the role of FGFR signaling in promoting motility in *VHL* knockdown HMVECs. Reduction of FGFR2 expression by specific siRNA in *VHL* knockdown HMVECs leads to significantly decreased cord-forming ability (Fig. 3*A*). Interestingly, knockdown of FGFR2 in *VHL*$^+$ cells to the same extent as in *VHL* knockdown cells (~ 3-fold) does not result in reduced cord formation, indicating that *VHL* knockdown cells are more reliant on FGFR signaling for their angiogenic activity. Further analysis of downstream signaling pathways revealed that, whereas Akt pathway remains unaffected (Supplementary Fig. S4*A*), ERK1/2 activity , measured by the levels of dp-ERK, is increased in *VHL* knockdown HMVECs. As shown in Fig. 3*B*, in *VHL* knockdown HMVECs, ERK1/2 activation is observed 5 min after pulsed bFGF induction. ERK1/2 activation reaches very high level at 20 min and is maintained through at least 60 min. In contrast, in *VHL*$^+$ cells, the initial levels of ERK1/2 activation are much reduced and the kinetics of signal activation is delayed. There is no activation at 5 min and modest activation at 20 to 60 min after receptor activation.

Next, we examined the specific role of ERK1/2 activation in promoting cell migration in *VHL* knockdown HMVECs. A widely used ERK signaling inhibitor PD98059 dramatically reduced ERK1/2 activation levels in FGF-induced *VHL* knockdown HMVECs (Fig. 3*C*). Concomitantly, *VHL* knockdown cells treated with PD98059 formed significantly fewer cords

than *VHL* knockdown cells treated with DMSO as control (Fig. 3*D*), to a level even lower than the wild-type DMSO-treated counterparts. Consistent with the FGFR2 knockdown results (Fig. 3*A*), cord formation by VHL^+ HMVECs was not affected by ERK inhibition (Fig. 3*D*), suggesting that alternative angiogenic pathways that are less dependent on ERK signaling may be used in wild-type endothelial cells. These cellular behaviors are similar to those described as "oncogene addiction," in which a cancer cell becomes overreliant on a pathologically overactivated oncogenic pathway (35). Thus, our results suggest that in *VHL* knockdown cells, FGFR-ERK signaling becomes the dominant angiogenic signaling pathway.

We have shown that *VHL* knockdown in HMVECs did not lead to increased Akt activation (Supplementary Fig. S4*A*). As expected, treatment with Akt inhibitor V, Triciribine, had no significant effect on cord formation by *VHL* knockdown HMVECs (Supplementary Fig. S4*B* and *C*).

Heterozygosity of *VHL* in mouse endothelial cells leads to increased angiogenic activity

To directly test our hypothesis that heterozygosity of *VHL* is a contributing factor in the hypervascularized phenotype in *VHL* tumors, we performed *in vivo* angiogenic assays in heterozygous *Vhl* knockout mice. In this assay, Matrigel embedded with or without bFGF was implanted s.c. in either $Vhl^{+/-}$ or the wild-type littermates. As shown in Fig. 4, although both $Vhl^{+/-}$ and wild-type mice exhibit low levels of angiogenesis without bFGF induction, $Vhl^{+/-}$ mice show a significantly higher response to bFGF than the wild-type counterparts. It is also noteworthy that the neovessels induced by bFGF in $Vhl^{+/-}$ show tortuous paths and irregular characteristics (e.g., variable diameters with frequent bulges and narrows), typical of tumor-induced vasculature. In contrast, bFGF-induced vessels in the wild-type animals are usually organized with smooth gradation of diameters. We also observed that $Vhl^{+/-}$ and wild-type mice responded equally well to VEGF-induced angiogenesis (data not shown).

To verify that the increased angiogenic response to bFGF is attributable to the endothelium, endothelial cells were isolated from wild-type and $Vhl^{+/-}$ renal cortex. After three rounds of purification using anti-CD31–conjugated magnetic beads, close to 100% of the cells express both CD31 and vWF (data not shown) and the $Vhl^{+/-}$ cells express <50% of the wild-type level of pVHL (Fig. 5*A*). These cells were then used in three-dimensional cord formation assay. As shown in Fig. 5*B*, $Vhl^{+/-}$ endothelial cells exhibit much higher capacity of cord formation than their wild-type counterparts.

ETS1 transcription factor is activated in *VHL* knockdown HMVECs

The ETS1 transcription factor is activated after ERK1/2 signaling in many cell types and is specifically expressed in endothelial cells undergoing tumor-induced and developmental angiogenesis (36,37). Also, the *in vivo* angiogenic effect of bFGF can be blocked by dominant-negative ETS1 construct (38). We therefore examined the role of ETS1 in *VHL* knockdown HMVECs. A direct measurement for ETS1 activity is to determine the phosphorylation levels at threonine (indicative of activation) or serine (indicative of inactivation) residues (39,40). Results of a pull-down assay (Fig. 6*A*) comparing VHL^+ and *VHL* knockdown lysates show greatly increased ETS1 threonine phosphorylation in *VHL* knockdown lysates at steady-state without acute bFGF induction (compare lanes 1 and 3). No significant changes in ETS1 serine phosphorylation were observed in *VHL* knockdown and control lysates with or without bFGF. As expected, bFGF induction of control cells resulted in increased ETS1 threonine phosphorylation to a level close to *VHL* knockdown cell without induction (compare lanes 1, 2, and 3), confirming the link between FGFR signaling and ETS1 activation, and consistent with the high intrinsic cord formation activity of the *VHL* knockdown cells (Fig. 1*D*). Induction with bFGF did not significantly increase the threonine phosphorylation level further in *VHL* knockdown cells (compare lanes 3 and 4). However, we consistently observed a decrease in

total ETS1 levels in *VHL* knockdown HMVECs stimulated with bFGF compared with unstimulated *VHL* knockdown HMVECs (compare lanes 7 and 8). Although the mechanism of ETS1 down-regulation is currently unknown, it nonetheless indicates that a much greater cellular fraction of the total ETS1 is activated in bFGF-stimulated *VHL* knockdown HMVECs.

Next, we examined the specific role of ETS1 activation in promoting motility in *VHL* knockdown HMVECs. We used an adenoviral ETS1-specific shRNA construct at 10 multiplicity of infection (MOI) to reduce expression of ETS1 in *VHL* knockdown and VHL^+ HMVECs (Fig. 6*B*, *left*). When ETS1 expression was reduced, migration of *VHL* knockdown HMVECs in transwell migration assay (Fig. 6*B*, *right*) and cord formation in three-dimensional coculture assay (Fig. 6*C*) were significantly reduced whereas cord formation by VHL^+ HMVECs was not affected, again supporting the notion that *VHL* mutant HMVECs preferentially rely on the FGFR signaling. In contrast, although knockdown of *VHL* results in an increase in the HIF-1α levels (Fig. 6*D*, *top left*), as expected, knockdown of HIF-1α in these cells did not impair their cord-forming activity (Fig. 6*D*, *bottom left* and *right*). Taken together, the elevated angiogenic activity of *VHL* knockdown endothelial cells is HIF independent and therefore likely not mediated by autocrine VEGF signaling loop.

Discussion

Our laboratory has previously reported that loss of function of the *Drosophila VHL* homologue resulted in ectopic migration and branching of *Drosophila* tracheal cells, a developmental model for angiogenesis, implying a direct role of *VHL* in mediating vascular cell motility *in vivo* (30). Recently, we showed that elevated motility in *VHL* null renal carcinoma cells is a direct consequence of cell surface accumulation of FGFR1 and enhanced signaling through ERK1/2 (16). In this report, we show that the FGFR-mediated signaling mechanism is conserved in the endothelial cell model. Using primary HMVECs, knockdown of *VHL* resulted in selective accumulation of FGFR2, leading to elevated angiogenic activity in response to fibroblasts or induced by bFGF through increased ERK1/2 signaling and ETS1 activity. Surface accumulation of FGFR is due to defective internalization of the activated receptor. This phenotype is selective because the effect does not extend to other receptor tyrosine kinases, such as VEGFR and EGFR. As shown in human RCC cells, pVHL selectively regulates FGFR endocytosis by stabilizing the endocytic activity of metastasis suppressor Nm23, which specifically associates with FGFR-containing endosomes but not EGFR-containing endosomes (16). Although the molecular mechanism involved in FGFR accumulation is likely similar in the previously reported RCC cells and in the endothelial cells reported here, our new findings are significant in at least three aspects.

First, our results with endothelial cells from heterozygous mice show that the *VHL* function in regulating FGFR signaling is haploid insufficient; that is, partial loss of *VHL* function (heterozygosity) can result in profound angiogenic phenotype, providing support for the notion that heterozygous *VHL* individuals may be more prone to hypervascularized tumors. Furthermore, we show that, whereas ERK signaling inhibitor had no effect on normal HMVEC cord formation activity, it greatly reduced that of the *VHL* knockdown cells to a level even lower than the wild-type untreated counterparts. This suggests that *VHL* knockdown cells become overreliant on bFGF stimulation for their angiogenic response and may provide a specific target for antiangiogenic intervention. In a broader implication, our findings also imply that spontaneous *VHL* mutations in the endothelium may contribute to vascular phenotypes in many lesions, including cancer.

Second, by using knockdown and knockout derivatives of normal primary endothelial cells, instead of reexpressing pVHL in cultured cancer cell lines, we are able to clearly define the

direct effect of *VHL* loss of function, without complication from other accumulated oncogenic modifications.

Third, in this report, we identified the transcription factor ETS1 as a major mediator of the elevated angiogenic activity in *VHL* mutant HMVECs. This should allow future studies to elucidate the specific angiogenic program that underlies the *VHL* mutant phenotype, using gene expression profiling based on the ETS1 activity.

We believe these findings are highly significant because the stromal compartment should be considered an integral part of the *VHL* tumorigenesis system. This is best illustrated by hemangioblastoma. Hemangioblastoma, uncontrolled vessel growth occurring in the central nervous system and retinas of VHL patients, is the most common VHL-associated tumor (41,42). Interestingly, because loss of heterozygosity of *VHL* is found only in cells neighboring the overgrown vessels (42–44), termed stromal cells, it is generally believed that the endothelium plays only a passive role in the disease, responding to the VEGF overproduced by the $VHL^{-/-}$ cells. However, this tumor is exceedingly rare in non-VHL patient population (45), suggesting that heterozygosity of the VHL patient endothelial cells may be a contributing factor. Our finding of elevated angiogenic activity in *VHL* loss-of-function endothelial cells is consistent with the previous report that a different strain of heterozygous *Vhl* mice developed spontaneous hemangioma-like lesions in the liver, but no other epithelial *VHL* tumors (18). Thus, it is likely that *VHL* mutant tumor cells (e.g., renal carcinoma cells and the stromal population of the hemangioblastoma lesions) do produce higher levels of angiogenic factors, such as VEGF, but partial loss of *VHL* in the endothelium also predisposes the tumor microenvironment to hypervascularization via elevated response to FGF that is secreted by the tumor cells or other stromal cells, such as fibroblasts. In light of the modest success using VEGF pathway antagonists in treating *VHL* mutant tumors (46–48), future improvements to the antiangiogenic therapy against VHL tumors should consider addition of specific FGF signaling antagonists or broader receptor tyrosine kinase blockers.

Supplementary Material

Refer to Web version on PubMed Central for supplementary material.

Acknowledgments

Grant support: NIH grants RO1CA109860 and PO1CA78582 (T. Hsu) and RO1CA128002 (V. Dammai) and Abney Scholarships for Cancer Research (K.J. Champion and M. Guinea).

We thank Dr. M. Trojanowska for providing valuable reagents.

References

1. Latif F, Tory K, Gnarra J, et al. Identification of the von Hippel-Lindau disease tumor suppressor gene. Science 1993;260:1317–1320. [PubMed: 8493574]
2. Lonser RR, Glenn GM, Walther M, et al. von Hippel-Lindau disease. Lancet 2003;361:2059–2067. [PubMed: 12814730]
3. Kaelin WG Jr. Molecular basis of the VHL hereditary cancer syndrome. Nat Rev Cancer 2002;2:673–682. [PubMed: 12209156]
4. Iwai K, Yamanaka K, Kamura T, et al. Identification of the von Hippel-lindau tumor-suppressor protein as part of an active E3 ubiquitin ligase complex. Proc Natl Acad Sci U S A 1999;96:12436–12441. [PubMed: 10535940]
5. Kamura T, Koepp DM, Conrad MN, et al. Rbx1, a component of the VHL tumor suppressor complex and SCF ubiquitin ligase. Science 1999;284:657–661. [PubMed: 10213691]

6. Lisztwan J, Imbert G, Wirbelauer C, Gstaiger M, Krek W. The von Hippel-Lindau tumor suppressor protein is a component of an E3 ubiquitin-protein ligase activity. Genes Dev 1999;13:1822–1833. [PubMed: 10421634]
7. Maxwell PH, Wiesener MS, Chang GW, et al. The tumour suppressor protein VHL targets hypoxia-inducible factors for oxygen-dependent proteolysis. Nature 1999;399:271–275. [PubMed: 10353251]
8. Kamura T, Sato S, Iwai K, et al. Activation of HIF1α ubiquitination by a reconstituted von Hippel-Lindau (VHL) tumor suppressor complex. Proc Natl Acad Sci U S A 2000;97:10430–10435. [PubMed: 10973499]
9. Maynard MA, Ohh M. Von Hippel-Lindau tumor suppressor protein and hypoxia-inducible factor in kidney cancer. Am J Nephrol 2004;24:1–13. [PubMed: 14654728]
10. Frew IJ, Krek W. Multitasking by pVHL in tumour suppression. Curr Opin Cell Biol 2007;19:685–690. [PubMed: 18006292]
11. Ohh M, Yauch RL, Lonergan KM, et al. The von Hippel-Lindau tumor suppressor protein is required for proper assembly of an extracellular fibronectin matrix. Mol Cell 1998;1:959–968. [PubMed: 9651579]
12. Kamada M, Suzuki K, Kato Y, Okuda H, Shuin T. von Hippel-Lindau protein promotes the assembly of actin and vinculin and inhibits cell motility. Cancer Res 2001;61:4184–4189. [PubMed: 11358843]
13. Hergovich A, Lisztwan J, Barry R, Ballschmieter P, Krek W. Regulation of microtubule stability by the von Hippel-Lindau tumour suppressor protein pVHL. Nat Cell Biol 2003;5:64–70. [PubMed: 12510195]
14. Koochekpour S, Jeffers M, Wang PH, et al. The von Hippel-Lindau tumor suppressor gene inhibits hepatocyte growth factor/scatter factor-induced invasion and branching morphogenesis in renal carcinoma cells. Mol Cell Biol 1999;19:5902–5912. [PubMed: 10454537]
15. Davidowitz EJ, Schoenfeld AR, Burk RD. VHL induces renal cell differentiation and growth arrest through integration of cell-cell and cell-extracellular matrix signaling. Mol Cell Biol 2001;21:865–874. [PubMed: 11154273]
16. Hsu T, Adereth Y, Kose N, Dammai V. Endocytic function of von Hippel-Lindau tumor suppressor protein regulates surface localization of fibroblast growth factor receptor 1 and cell motility. J Biol Chem 2006;281:12069–12080. [PubMed: 16505488]
17. Tang N, Mack F, Haase VH, Simon MC, Johnson RS. pVHL function is essential for endothelial extracellular matrix deposition. Mol Cell Biol 2006;26:2519–2530. [PubMed: 16537898]
18. Haase VH, Glickman JN, Socolovsky M, Jaenisch R. Vascular tumors in livers with targeted inactivation of the von Hippel-Lindau tumor suppressor. Proc Natl Acad Sci U S A 2001;98:1583–1588. [PubMed: 11171994]
19. Kleymenova E, Everitt JI, Pluta L, et al. Susceptibility to vascular neoplasms but no increased susceptibility to renal carcinogenesis in Vhl knockout mice. Carcinogenesis 2004;25:309–315. [PubMed: 14604887]
20. Kondo K, Kim WY, Lechpammer M, Kaelin WG Jr. Inhibition of HIF2α is sufficient to suppress pVHL-defective tumor growth. PLoS Biol 2003;1:E83. [PubMed: 14691554]
21. Sowter HM, Raval RR, Moore JW, Ratcliffe PJ, Harris AL. Predominant role of hypoxia-inducible transcription factor (Hif)-1α versus Hif-2α in regulation of the transcriptional response to hypoxia. Cancer Res 2003;63:6130–6134. [PubMed: 14559790]
22. Velazquez OC, Snyder R, Liu ZJ, Fairman RM, Herlyn M. Fibroblast-dependent differentiation of human microvascular endothelial cells into capillary-like 3-dimensional networks. FASEB J 2002;16:1316–1318. [PubMed: 12060671]
23. Chintalapudi MR, Markiewicz M, Kose N, et al. Cyr61/CCN1 and CTGF/CCN2 mediate the pro-angiogenic activity of VHL mutant renal carcinoma cells. Carcinogenesis 2008;29:696–703. [PubMed: 18212329]
24. Gnarra JR, Ward JM, Porter FD, et al. Defective placental vasculogenesis causes embryonic lethality in VHL-deficient mice. Proc Natl Acad Sci U S A 1997;94:9102–9107. [PubMed: 9256442]
25. Richard L, Velasco P, Detmar M. A simple immunomagnetic protocol for the selective isolation and long-term culture of human dermal microvascular endothelial cells. Exp Cell Res 1998;240:1–6. [PubMed: 9570915]

26. Akis N, Madaio MP. Isolation, culture, and characterization of endothelial cells from mouse glomeruli. Kidney Int 2004;65:2223–2227. [PubMed: 15149335]
27. Gazzaniga S, Gonzalez L, Mantovani A, Vecchi A, Wainstok R. Isolation and molecular characterization of a mouse renal microvascular endothelial cell line. *In vitro* Cell Dev Biol Anim 2004;40:82–88. [PubMed: 15311962]
28. Grant MB, Khaw PT, Schultz GS, Adams JL, Shimizu RW. Effects of epidermal growth factor, fibroblast growth factor, and transforming growth factor-β on corneal cell chemotaxis. Invest Ophthalmol Vis Sci 1992;33:3292–3301. [PubMed: 1428704]
29. Liu X, Lin CS, Graziottin T, Resplande J, Lue TF. Vascular endothelial growth factor promotes proliferation and migration of cavernous smooth muscle cells. J Urol 2001;166:354–360. [PubMed: 11435899]
30. Adryan B, Decker HJ, Papas TS, Hsu T. Tracheal development and the von Hippel-Lindau tumor suppressor homolog in Drosophila. Oncogene 2000;19:2803–2811. [PubMed: 10851083]
31. Dammai V, Adryan B, Lavenburg KR, Hsu T. Drosophila awd, the homolog of human nm23, regulates FGF receptor levels and functions synergistically with shi/dynamin during tracheal development. Genes Dev 2003;17:2812–2824. [PubMed: 14630942]
32. Hsouna A, Lawal HO, Izevbaye I, Hsu T, O'Donnell JM. Drosophila dopamine synthesis pathway genes regulate tracheal morphogenesis. Dev Biol 2007;308:30–43. [PubMed: 17585895]
33. Suyama K, Shapiro I, Guttman M, Hazan RB. A signaling pathway leading to metastasis is controlled by N-cadherin and the FGF receptor. Cancer Cell 2002;2:301–314. [PubMed: 12398894]
34. Wiley HS, Burke PM. Regulation of receptor tyrosine kinase signaling by endocytic trafficking. Traffic 2001;2:12–18. [PubMed: 11208164]
35. Weinstein IB, Joe AK. Mechanisms of disease: oncogene addiction-a rationale for molecular targeting in cancer therapy. Nat Clin Pract Oncol 2006;3:448–457. [PubMed: 16894390]
36. Rabault B, Roussel MF, Quang CT, Ghysdael J. Phosphorylation of Ets1 regulates the complementation of a CSF-1 receptor impaired in mitogenesis. Oncogene 1996;13:877–881. [PubMed: 8761310]
37. Wernert N, Raes MB, Lassalle P, et al. c-ets1 protooncogene is a transcription factor expressed in endothelial cells during tumor vascularization and other forms of angiogenesis in humans. Am J Pathol 1992;140:119–127. [PubMed: 1370594]
38. Pourtier-Manzanedo A, Vercamer C, Van Belle E, et al. Expression of an Ets-1 dominant-negative mutant perturbs normal and tumor angiogenesis in a mouse ear model. Oncogene 2003;22:1795–1806. [PubMed: 12660815]
39. Yang BS, Hauser CA, Henkel G, et al. Ras-mediated phosphorylation of a conserved threonine residue enhances the transactivation activities of c-Ets1 and c-Ets2. Mol Cell Biol 1996;16:538–547. [PubMed: 8552081]
40. Yordy JS, Muise-Helmericks RC. Signal transduction and the Ets family of transcription factors. Oncogene 2000;19:6503–6513. [PubMed: 11175366]
41. Welch RB. Von Hippel-Lindau disease: the recognition and treatment of early angiomatosis retinae and the use of cryosurgery as an adjunct to therapy. Trans Am Ophthalmol Soc 1970;68:367–424. [PubMed: 5535648]
42. Chan CC, Vortmeyer AO, Chew EY, et al. VHL gene deletion and enhanced VEGF gene expression detected in the stromal cells of retinal angioma. Arch Ophthalmol 1999;117:625–630. [PubMed: 10326959]
43. Vortmeyer AO, Gnarra JR, Emmert-Buck MR, et al. von Hippel-Lindau gene deletion detected in the stromal cell component of a cerebellar hemangioblastoma associated with von Hippel-Lindau disease. Hum Pathol 1997;28:540–543. [PubMed: 9158701]
44. Vortmeyer AO, Tran MG, Zeng W, et al. Evolution of VHL tumourigenesis in nerve root tissue. J Pathol 2006;210:374–382. [PubMed: 16981244]
45. Woodward ER, Wall K, Forsyth J, Macdonald F, Maher ER. VHL mutation analysis in patients with isolated central nervous system haemangioblastoma. Brain 2007;130:836–842. [PubMed: 17264095]
46. Yang JC, Haworth L, Sherry RM, et al. A randomized trial of bevacizumab, an anti-vascular endothelial growth factor antibody, for metastatic renal cancer. N Engl J Med 2003;349:427–434. [PubMed: 12890841]

47. Reuter CW, Morgan MA, Grunwald V, et al. Targeting vascular endothelial growth factor (VEGF)-receptor-signaling in renal cell carcinoma. World J Urol 2007;25:59–72. [PubMed: 17340158]

48. Srinivasan R, Armstrong AJ, Dahut W, George DJ. Anti-angiogenic therapy in renal cell cancer. BJU Int 2007;99:1296–1300. [PubMed: 17441927]

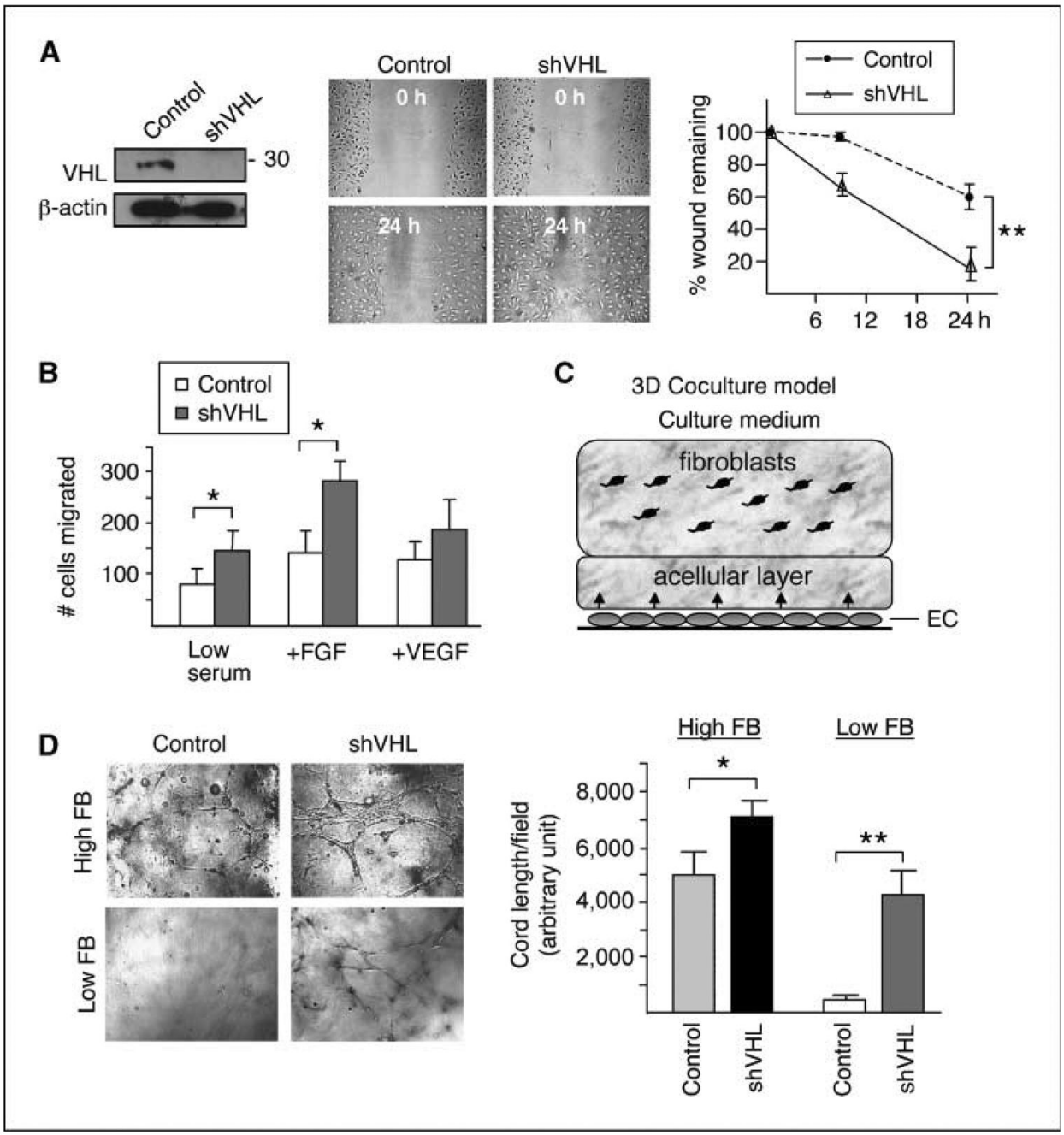

Figure 1.

Knockdown of *VHL* increases cell motility in HMVECs. *A, left*, HMVECs were transfected with vectors expressing control shRNA or *VHL* shRNA constructs (*shVHL*). Cell lysates were Western blotted using VHL antibody or β-actin antibody as a loading control. The apparent molecular weight of the detected pVHL species (~ 30 kDa) is indicated. *Middle*, 90% confluent cell monolayers in six-well culture dishes were scratched with a 1,000-μL pipette tip. Wound healing was followed in control and *VHL* knockdown HMVECs for 24 h. *Right*, extent of wound healing was quantified in control and *VHL* knockdown HMVECs by measuring percentage of wound remaining over time using NIH ImageJ software ($n = 3$). *B*, quantification of transwell assays for intrinsic (low serum) and chemotactic (+FGF and +VEGF) cell

migration over 24 h for control and *VHL* knockdown HMVECs ($n = 5$). *C*, schematic representation of the three-dimensional coculture system. Cord formation by the HMVECs is supported by stromal cells, such as human dermal fibroblasts, and can be observed within 72 h by confocal microscopy usually at a depth of ~ 100 μm from the bottom of the well. *D*, *left*, images taken inside collagen gel of control and *VHL* knockdown HMVECs cocultured with high (3.75×10^4 per chamber) or low (1.5×10^4 per chamber) amount of fibroblasts (*FB*). *Right*, Cord formation by control and *VHL* knockdown HMVECs cocultured with high (*first and second columns*) or low (*third and fourth columns*) amount of fibroblasts was quantified using NIH ImageJ software to measure total cord length per field. Assay was performed in triplicate chambers for each condition. Random fields containing cord formation were chosen for quantification from each condition. Statistical analysis was performed using Student's *t* test ($n = 9$ for high fibroblast condition, $n = 3$ for low fibroblast condition). *, $P \leq 0.05$; **, $P \leq 0.01$.

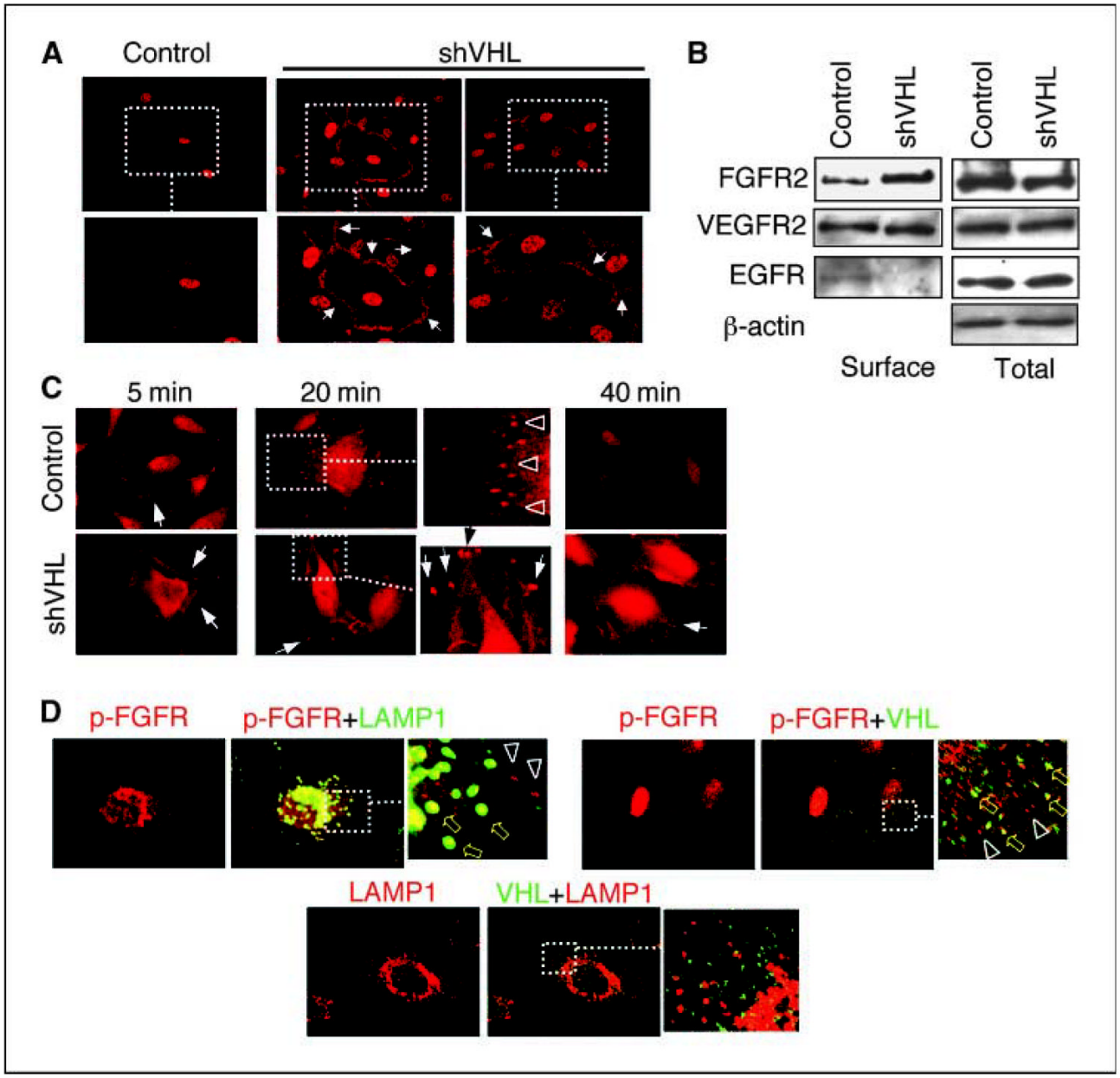

Figure 2.

Surface accumulation of FGFR in *VHL* knockdown HMVECs. *A*, HMVECs transfected with plasmids expressing either control or *VHL* shRNA (*shVHL*) were incubated in complete serum with growth factor supplements and processed for immunostaining with anti–p-FGFR antibody. High levels of surface accumulation of p-FGFR (*arrows*) are observed in *VHL* knockdown HMVECs (*shVHL*) but not in control cells. *B*, control and *VHL* knockdown HMVECs (*shVHL*) are labeled with membrane-impermeable sulfo-NHS-LC biotin at 4°C. Samples were immunoprecipitated using NeutrAvidin biotin-binding protein and surface receptor levels detected using indicated antibodies. Total receptor levels were detected from total input lysates (1/12 of the amount used in pull-down) using indicated antibodies. *C*, ligand-stimulated endocytosis of activated FGFR was synchronized and followed over time. Serum-starved cells were incubated with bFGF + heparin at 4°C for 2 h and then chased with ligand-

free media at 37°C over a 40-min period. Arrows denote p-FGFR visible at or near the cell surface at 5 min. Arrowheads in control inset (20 min) denote p-FGFR that is internalized into intracellular vesicles. Arrows in *VHL* knockdown (20 and 40 min) denote p-FGFR appearing in large aggregates at the tips of cellular projections. *D*, ligand-stimulated endocytosis of activated FGFR was synchronized and followed for 20 min in control HMVECs. Triplicate wells were double-stained for p-FGFR/LAMP1, p-FGFR/VHL, and LAMP1/VHL, as indicated. *Top left*, p-FGFR (*red*) and LAMP1 (*green*) colocalize in some vesicles (*yellow block arrows*), whereas others contain only p-FGFR (*arrowheads*). *Top right*, VHL (*green*) and p-FGFR (*red*) colocalize in some vesicles (*yellow block arrows*) but not others (*arrowheads*). *Bottom*, VHL (*green*) does not overlap with LAMP1 (*red*).

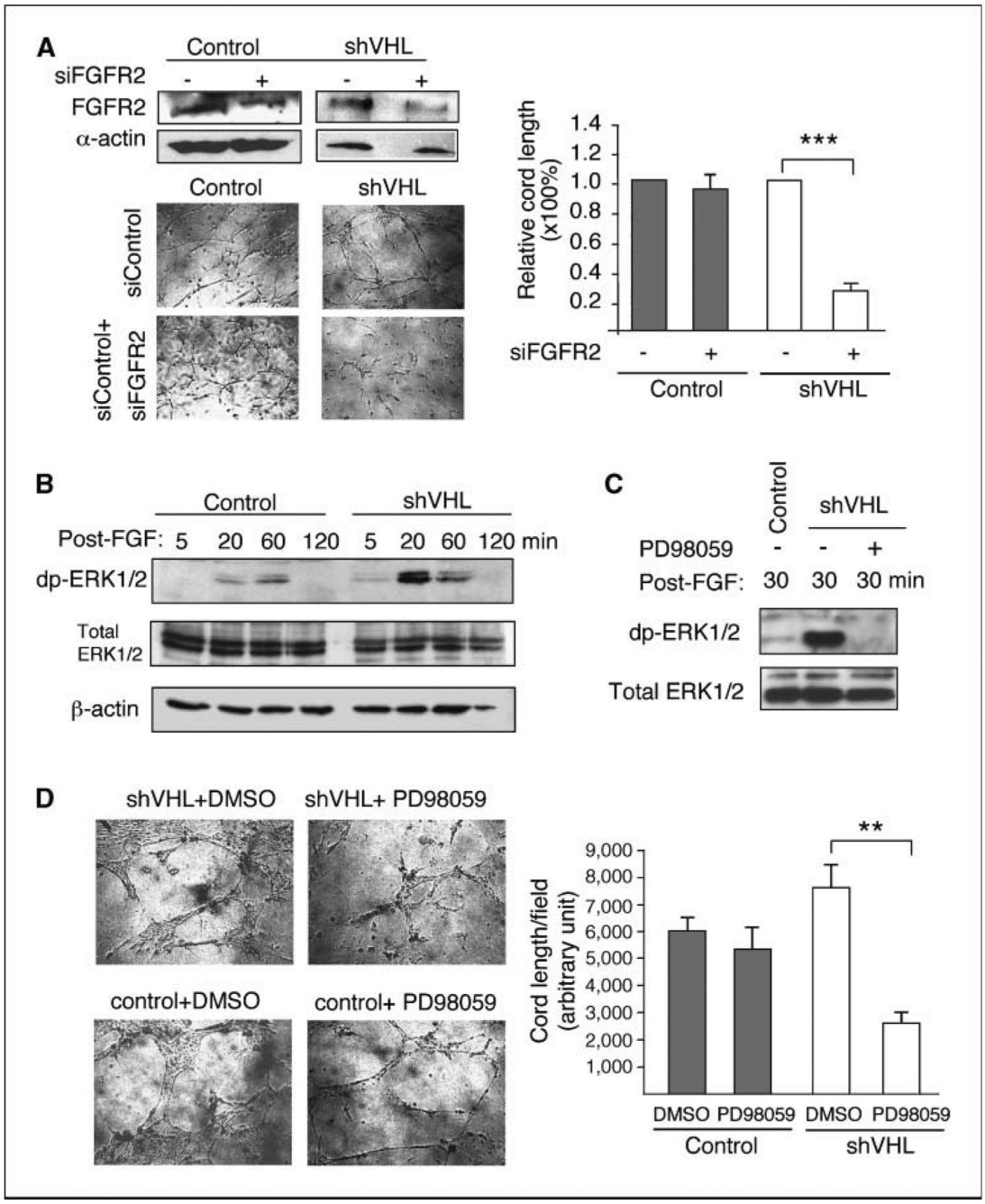

Figure 3.

ERK1/2 pathway mediates cord formation by *VHL* knockdown HMVECs. *A*, *top left*, transfection of FGFR2 siRNA (siFGFR2) reduces expression of FGFR2 protein in both control and *VHL* knockdown HMVECs by ~ 3-fold. *Bottom left* and *right*, knockdown of FGFR2 (siFGFR2) expression significantly reduces cord formation by *VHL* knockdown HMVECs (shVHL) placed in three-dimensional coculture assay under high fibroblast condition, but has little effect on the control cells. *B*, kinetics of ERK1/2 activation in control and *VHL* (*shVHL*) knockdown cells stimulated with bFGF and heparin and chased for 5, 20, 60, or 120 min (post-FGF) as described in Fig. 2*C*. ERK1/2 activation was measured by the levels of dp-ERK. Total ERK1/2 and β-actin were used as loading controls. *C*, *VHL* knockdown HMVECs

(*shVHL*) were incubated with 25 μmol/L PD98059 (+) or DMSO (−) for 4 h and then treated with bFGF and heparin followed by ligand-free chase as described in Fig. 2*C*. Lysates were collected at 30 min after chase. ERK1/2 activation is ameliorated by PD98059 as measured by levels of dp-ERK. *D*, treatment of *VHL* knockdown HMVECs (*shVHL*) with 25 μmol/L PD98059 significantly reduces cord formation in three-dimensional coculture assay in the presence of high amount of fibroblasts. Statistical analysis was performed using Student's *t* test ($n = 4$). **, $P \leq 0.01$; ***, $P \leq 0.001$.

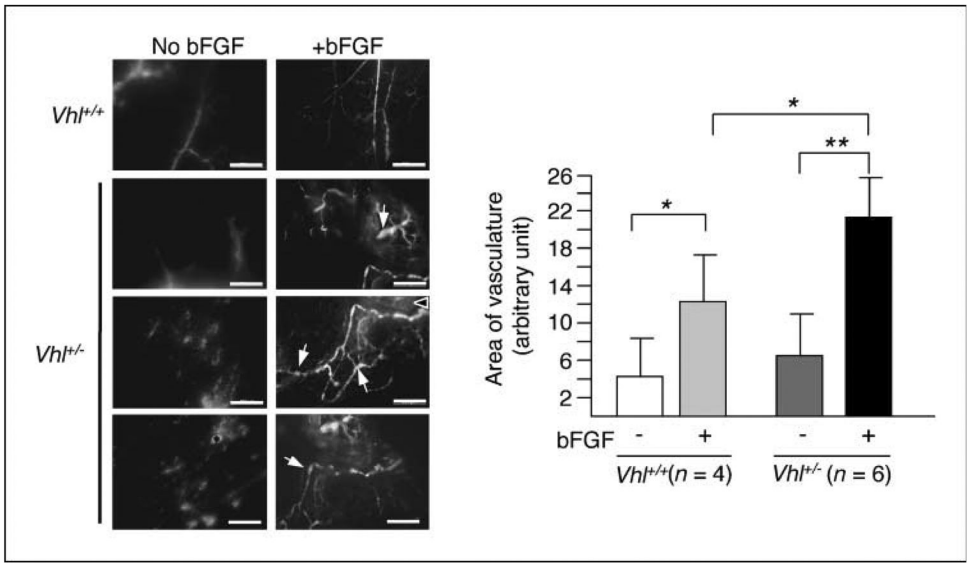

Figure 4.

Vhl-heterozygous animals show increased neoangiogenic response to bFGF. $Vhl^{+/-}$ mice or the wild-type littermates were injected s.c. with Matrigel with or without embedded bFGF. Seven days after gel implantation, FITC-dextran was infused by intracardiac injection. The gel was dissected 10 min later. Compared with wild-type, bFGF-loaded Matrigel plug in $Vhl^{+/-}$ induces more abundant neovessels with tortuous and chaotic patterns. Arrows point to examples of bulges typically found in bFGF-induced $Vhl^{+/-}$ vessels. Scale bars, 200 μm. Quantification of the area covered by vessels was performed by measuring the fluorescent area of each picture containing vessels using NIH ImageJ software. The angiogenic response to bFGF is more robust in $Vhl^{+/-}$ mice ($n = 6$) than in the wild-type counterpart ($n = 4$). Statistical analysis was performed using Student's *t* test. *, $P \leq 0.05$; **, $P \leq 0.01$.

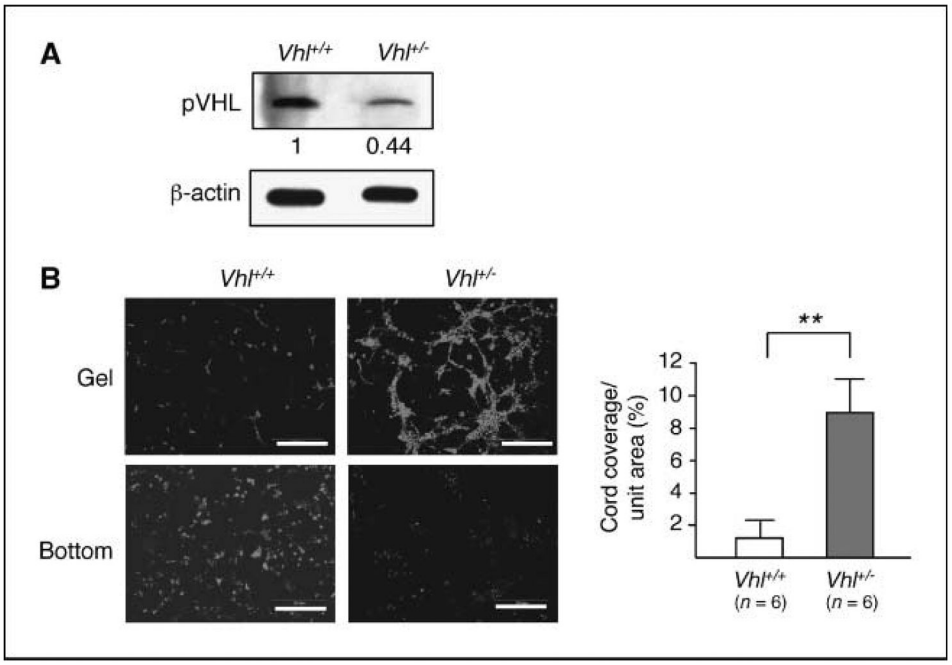

Figure 5.

Increased level of cord formation by $Vhl^{+/-}$ mouse endothelial cells. Isolated mouse kidney cortical endothelial cells from $Vhl^{+/-}$ and the wild-type littermates were assayed in the three-dimensional coculture system as described in Fig. 1. *A*, Western analysis of the cell lysates shows a >50% decrease of pVHL level in the $Vhl^{+/-}$ cells compared with the wild type. *B*, the endothelial cells were preincubated with live dye CM-Dil. Images were taken at ~ 100 to 150 μm from the bottom of the well (Gel) as well as at the bottom. $Vhl^{+/-}$ cells show high levels of cord formation with few remaining at the bottom, whereas wild-type cells mostly remain at the bottom. *Scale bars*, 200 μm. The angiogenic activity was measured by unit area covered by networks of $Vhl^{+/-}$ ($n = 6$) and wild-type ($n = 6$) mouse kidney endothelial cells. Statistical analysis was performed using Student's *t* test. **, $P \leq 0.01$.

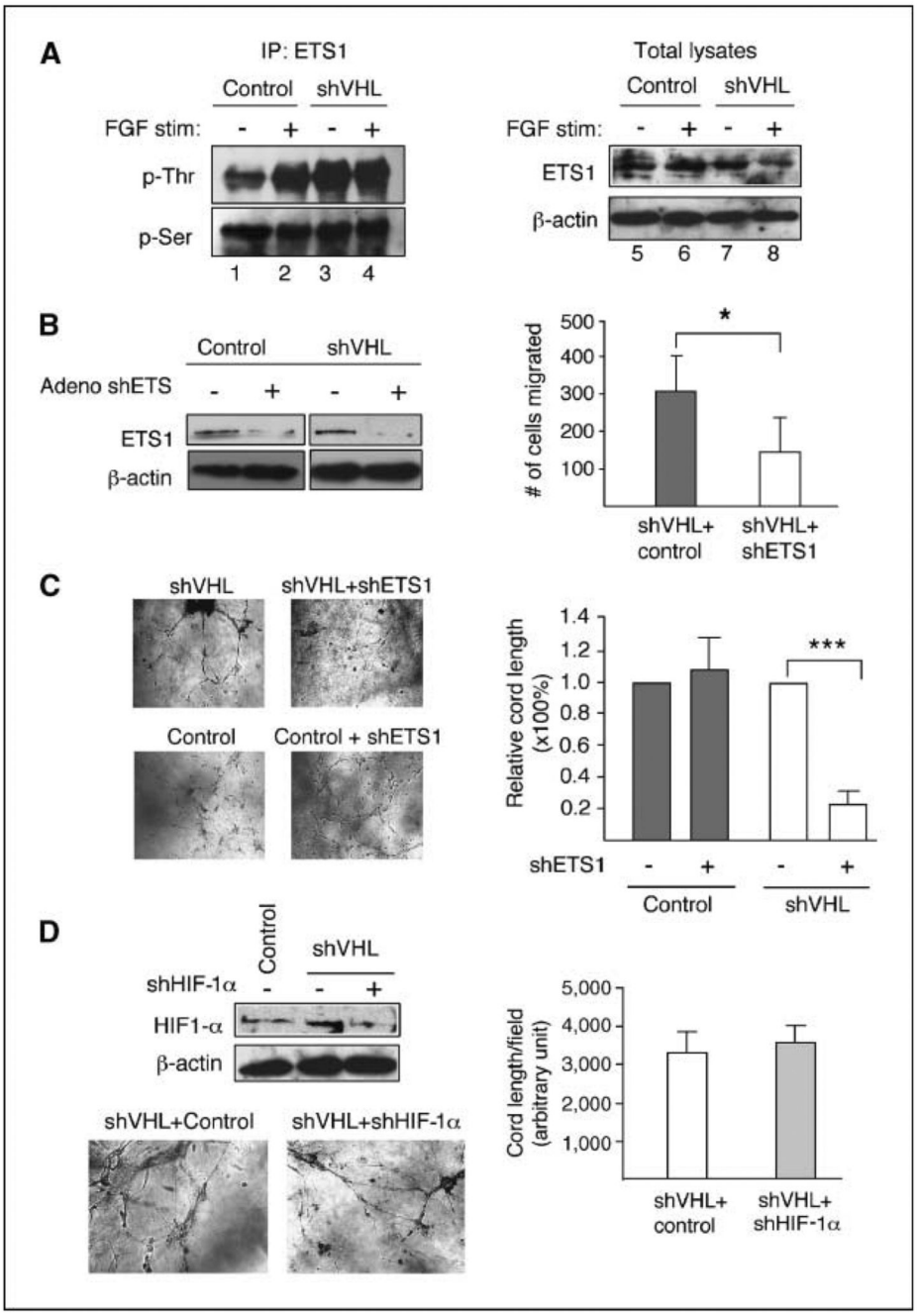

Figure 6.

ETS1 transcription factor mediates angiogenic activity of *VHL* knockdown HMVECs. *A*, control or *VHL* knockdown (*shVHL*) lysates (1 mg) stimulated with (*lanes 2 and 4*) or withou t (*lanes 1 and 3*) bFGF + heparin are incubated with ETS1 antibody and pull-down performed with protein G–sepharose beads. Pulled-down fractions are probed with phosphothreonine (*p-Thr*) and reprobed with phosphoserine (*p-Ser*) antibodies. Total lysates (100 μg) from control or *VHL* knockdown HMVECs stimulated with (*lanes 6 and 8*) or without (*lanes 5 and 7*) bFGF are probed with ETS1 antibody and reprobed with β-actin for loading control. *B*, *left*, treatment of *VHL* knockdown HMVECs (*shVHL*) with 10 MOI of ETS1-specific adeno shRNA (+) reduces ETS1 expression compared with treatment with control (−) virus. *Right*, transwell

migration assay for *VHL* knockdown HMVECs treated with 10 MOI of control virus (*shVHL + control*) or 10 MOI of ETS1-specific adeno siRNA (*shVHL + shETS1*). Statistical analysis was performed using Student's *t* test ($n = 4$). *C*, knockdown of ETS1 expression by 10 MOI ETS1-specific adeno siRNA significantly reduces cord formation by *VHL* knockdown HMVECs but has no effect on control cells. *D, top left*, HIF-1α expression in *VHL* wild-type (control shRNA), *VHL* single knockdown, and *VHL-HIF-1α* double knockdown cells. *Bottom left*, cord formation assay comparing *VHL* single knockdown (*shVHL + control*) and *VHL-HIF-1α* double knockdown (*shVHL + shHIF-1α*). *Right*, quantification of cord formation assay shown on the left. Statistical analysis was performed using Student's *t* test ($n = 4$). *, $P \leq 0.05$; ***, $P \leq 0.001$.